THE JOURNAL OF BIOLOGICAL CHEMISTRY VOL. 287, NO. 8, pp. 5290–5300, February 17, 2012

Axonal Gradient of Arachidonic Acid-containing Phosphatidylcholine and Its Dependence on Actin Dynamics*

Received for publication, October 24, 2011, and in revised form, December 27, 2011 Published, JBC Papers in Press, December 29, 2011, DOI 10.1074/jbc.M111.316877

Hyun-Jeong Yang[1], **Yuki Sugiura**[2], **Koji Ikegami, Yoshiyuki Konishi**[3], **and Mitsutoshi Setou**[4]

From the Department of Cell Biology and Anatomy, Hamamatsu University School of Medicine, 1-20-1, Handayama, Hamamatsu 431-3192, Japan

Background: The neuronal distribution of arachidonic acid-containing phosphatidylcholine (AA-PC) remains unknown.
Results: AA-PC axonal intensity showed a proximal-to-distal gradient, which was disrupted by actin inhibitors.
Conclusion: AA-PC occupies a higher portion of PC at distal than at proximal axons and may be associated with actin dynamics.
Significance: This research provides a better understanding of the neuronal spatial composition of PC.

Phosphatidylcholine (PC) is the most abundant component of lipid bilayers and exists in various molecular forms, through combinations of two acylated fatty acids. Arachidonic acid (AA)-containing PC (AA-PC) can be a source of AA, which is a crucial mediator of synaptic transmission and intracellular signaling. However, the distribution of AA-PC within neurons has not been indicated. In the present study, we used imaging mass spectrometry to characterize the distribution of PC species in cultured neurons of superior cervical ganglia. Intriguingly, PC species exhibited a unique distribution that was dependent on the acyl chains at the *sn*-2 position. In particular, we found that AA-PC is enriched within the axon and is distributed across a proximal-to-distal gradient. Inhibitors of actin dynamics (cytochalasin D and phallacidin) disrupted this gradient. This is the first report of the gradual distribution of AA-PC along the axon and its association with actin dynamics.

Arachidonic acid (AA)[5] mediates several crucial functions such as neuronal firing (1, 2), signaling (3), and long term potentiation (4). Phosphatidylcholine (PC) is a class of lipids and a major component of most intracellular membranes. It is composed of a choline head group, a phosphoglycerol backbone, and two acyl chains of various combinations, which generate various PC species. PC is synthesized by a *de novo* pathway (Kennedy pathway) and maintained by a remodeling pathway (Lands cycle) (5). Some intracellular bilayers include PC containing AA (AA-PC) (6), and actin dynamics have been known to mediate bilayer movement (7–9). However, the distribution of AA-PC within the neuron and its relationship with actin dynamics are not well known.

There have been attempts to visualize lipids. Recently, imaging mass spectrometry has been applied to lipid research, providing an opportunity to visualize endogenous lipids by their specific molecular weights. At a tissue level, we visualized intact PC distributions by matrix-assisted laser/desorption ionization (MALDI) with minimal fragmentation (10). However, the PC distribution has not been characterized by MALDI at an intracellular level. An elegant MALDI experiment measured signaling peptides in rat pituitary cells (11, 12). In addition, time-of-flight secondary-ion mass spectrometry (TOF-SIMS) has been used to characterize cell surface PC fragments at a single-cell level, revealing low distribution of the PC head group at the membrane fusion site of *Tetrahymena* (13) and high distribution of the PC head group at the nuclear membrane in blood cells (14). Although TOF-SIMS provides valuable information about the PC head group, it is difficult to distinguish intact PC species because of high fragmentation.

To visualize intrinsic neuronal PC at an intracellular level, we employed MALDI-imaging, wherein PC molecules can be detected with less fragmentation. Measurements were performed on explant cultures of mouse superior cervical ganglia (SCG). We found that PC showed a characteristic distribution depending on the acyl chains at the *sn*-2 position. Specifically, AA-PC exhibited a gradient of increasing intensity along the proximodistal axonal axis. Intriguingly, this characteristic distribution of AA-PC was disrupted by the inhibition of actin dynamics, indicating that the AA-PC distribution is dependent on actin dynamics.

EXPERIMENTAL PROCEDURES

Cultures—Procedures for the use and care of animals were compliant with the guidelines set forth by the Institutional Animal Care and Use Committee at Hamamatsu University School of Medicine. Cultures were performed and grown as reported

* This work was supported by a grant-in-aid for SENTAN (Development of Systems and Technology for Advanced Measurement and Analysis) from the Japanese Science and Technology Agency, Wakate S, and Tokutei (to M. S.). The "Lipid Machineries" research was supported by Monbu Kagakusho.

[1] Present address: Dept. of Molecular Cell Biology, Weizmann Institute of Science, 76100 Rehovot, Israel.
[2] Present address: Dept. of Biochemistry, School of Medicine, Keio University, Shinanomachi 35, Tokyo 160-8582, Japan.
[3] Present address: Graduate School of Engineering, and Research and Education Program for Life Science, University of Fukui, 3-9-1 Bunkyo, Fukui 910-8507, Japan.
[4] To whom correspondence should be addressed. Tel.: 81-53-435-2292; Fax: 81-53-435-2292; E-mail: setou@hama-med.ac.jp.

[5] The abbreviations used are: AA, arachidonic acid; AA-PC, AA-containing PC; calcein-AM, calcein-acetoxymethyl ester; cPLA, cytosolic phospholipase; DHA, docosahexaenoic acid; DIV, day *in vitro*; F-actin, filamentous actin; G-actin, globular actin; iPLA, calcium-independent phospholipase; *k*, axonal slope coefficient index; LC-ESI-MS/MS, liquid chromatography-electrospray ionization-tandem MS; LA, linoleic acid; LCPUFA, long chain polyunsaturated fatty acid; MUSA, monounsaturated fatty acid; PC, phosphatidylcholine; SA, saturated fatty acid; SCG, superior cervical ganglia; TOF-SIMS, time-of-flight secondary-ion mass spectrometry.

previously (15), with modifications for performing MALDI-imaging (16). Briefly, SCG dissected from P0 ICR mice, following careful removal of other cell types, were cut into halves, each of which contained ~15,000 neuronal cell bodies (17). The SCG were placed on indium-tin-oxide glass slides (Bruker Daltonics, Leipzig, Germany), to which flexiperms were attached. The slides were coated with 1 mg/ml poly-L-lysine, followed by 10 μg/ml laminin. The cells were grown in fresh feeding medium under the following conditions: 10% FBS /minimum essential medium supplemented with 50 ng/ml nerve growth factor; 15 μM fluorodeoxyuridine, and 15 μM uridine at 37 °C in a humidified atmosphere of 5% CO_2/95% air. On the following day, the anti-mitotic drug aphidicolin (6 μM) was added to eliminate non-neuronal cells. Neurons were grown in the feeding medium for 4–5 days prior to each experiment.

Immunostaining and Labeling with Calcein-Acetoxymethyl Ester (AM)—Cultured SCG neurons were fixed with 4% paraformaldehyde diluted in phosphate-buffered saline (PBS) for 20 min at room temperature, washed with 1× PBS, and permeabilized with 0.1% Triton X-100/PBS for 10 min. The cells were then blocked with blocking reagent (5% goat/1% BSA/0.1% NaN_3/PBS) for 1 h and incubated with the primary antibody diluted in blocking reagent overnight at 4 °C. After washing, the cells were incubated with Alexa Fluor 488- or 568-conjugated anti-mouse IgG antibody (Molecular Probes, Eugene, OR) diluted with blocking reagent at room temperature for 1 h, then washed with 1× PBS. For nuclear staining, TOTO-3 (Molecular Probes) was added at the washing step after the secondary antibody. For actin staining, the same procedures were used, but the cells were fixed at 37 °C and incubated with 6.6 μM Alexa Fluor 488 phalloidin (Molecular Probes) for 1 h at 37 °C. The following mouse monoclonal antibodies were used: anti-Tau-1 (Chemicon, Temecula, CA), MAP2, and DM1A for α-tubulin staining (Sigma-Aldrich). Observations and image creations were carried out with a confocal microscope (FluoView1000; Olympus, Tokyo, Japan). For calcein-AM labeling (Dojindo, Kumamoto, Japan), SCG neurons were incubated with 500 nM calcein-AM diluted in medium for 1 h at 37 °C in the dark. Observations and image creations were carried out with the Aqua Cosmos image acquisition and analysis system for microscopy (Hamamatsu Photonics, Hamamatsu, Japan).

Inhibitor Treatment—SCG neurons collected at 4–5 days *in vitro* (DIV) were treated for 2 h with the following inhibitors or vehicles using the same amount of organic solvent that was used for inhibitor dissolution: 78.8 μM cytochalasin D, 25 μM phallacidin, 33.2 μM nocodazole, 1 μM cytosolic phospholipase (cPLA) 2α inhibitor, 10 μM bromoenol lactone, or 10 μM blebbistatin. Cytochalasin D, phallacidin, and nocodazole were purchased from Sigma-Aldrich; cPLA2α inhibitor and blebbistatin were purchased from Calbiochem. Bromoenol lactone was purchased from Cayman (Ann Arbor, MI).

Sample Preparation—For MALDI-imaging, sample preparation was performed as described previously (16). Briefly, cultures were washed rapidly and then immediately frozen on dry ice. After drying in a vacuum chamber for 3 h, 2,5-dihydroxybenzoic acid (Bruker Daltonics) matrix solution (50 mg/ml diluted in 70% methanol, 20 mM potassium acetate, and ultrapure water) was applied to the sample. For sample preparation of MALDI-mass spectrometry (MS) and liquid chromatography (LC)-electrospray ionization (ESI)-tandem MS (MS/MS), the freeze-dried cells were subjected to laser-capture microdissection (Leica Laser Microdissection LMD6000, Leica Microsystems, Inc., Germany) to divide the neurons into cell bodies and axonal parts. Samples were laser-detached from indium-tin-oxide slide glasses, harvested into tubes, and dissolved in methanol.

Measurement—For MALDI-imaging and MALDI-MS/MS, measurements were performed using a MALDI TOF/TOF-type instrument (Ultraflex 2 TOF/TOF; Bruker Daltonics) as described previously (16), with minor modifications. The instrument was equipped with a 355-nm Nd:YAG laser. Data were acquired in the positive reflectron mode under an accelerating potential of 25 kV by using an external calibration method. Signals between m/z 700 and m/z 1000 were collected. The raster size was 30 μm. Image reconstruction was performed using FlexImaging 2.0 software (Bruker Daltonics). LC-ESI-MS/MS measurements were performed using a 4000Q-TRAP quadrupole linear ion trap hybrid mass spectrometer (Applied Biosystems/MDS Sciex, Concord, ON, Canada) with ACQUITY Ultra Performance Liquid Chromatography® (Waters, Milford, MA). The samples were resolved on an ACQUITY UPLCTM BEH C18 column (1.0 × 150-mm inner diameter, 0.17-μm particle) and subjected directly to ESI-MS/MS analysis (10).

Image Analyses—The imaging MS data were opened in FlexImaging 2.0 software. Each data point was normalized by total ion current to eliminate variation of ionization efficiency. To present data by PC component and to minimize noise, the data were loaded into Analysis Software for Shimadzu Imaging Mass Spectrometry (Shimadzu, Kyoto, Japan) and normalized by the sum of the ion currents of the major PC species. To analyze axonal parts, the data were further processed in Tissue view (Applied Biosystems). We divided the entire axonal region into five subregions and used four axonal regions for analysis. In each region, we averaged the MS signal intensities of each PC from every pixel and plotted the average signal values. Analytical details are described in Fig. 3.

RESULTS

AA-PC Levels Were Higher in Axon Than in Cell Body—Throughout the study, we utilized explant cultures of SCG neurons to analyze and compare distinctive intracellular PC distributions within the cell body and axons. This was facilitated by the highly polarized and simple morphology of SCG explant cultures, consisting of a cell body mass (TOTO-3-positive) and axons (Tau1-positive and MAP2-negative) (Fig. 1*A*). There are many different PC molecular species with various combinations of two acyl chains (Fig. 1*B*). Initially, to investigate the overall PC molecular species composition in SCG neurons, we directly analyzed the neuronal culture by MALDI-MS and MS/MS. We detected ions of several PC molecular species and identified them by MS/MS (Table 1) by detecting the trimethylamine head group, *i.e.* choline (m/z 59) and/or phosphate (m/z 124) in the MS/MS product ion mass spectra (10).

Next, we investigated whether the composition of PC molecular species differed between the cell body and axon. Each com-

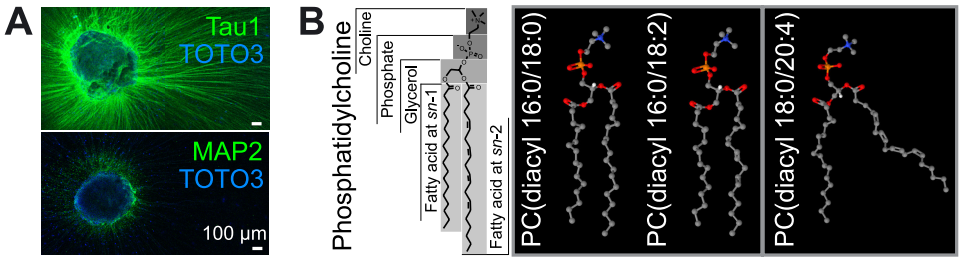

FIGURE 1. **Major PC species in axons of mouse SCG neurons.** *A*, immunostaining of SCG neurons with axonal marker Tau1, dendritic marker MAP2, and nuclear marker TOTO-3. *Scale bars*, 100 μm. *B*, schemes for PC species. Acyl chain information of PC is written as follows: PC(diacyl-[fatty acid at *sn*-1]/[fatty acid at *sn*-2]). Expected structures were visualized using Jmol viewer (48) based on a previous report (49).

TABLE 1
Results of MS and MS^n with the intense mass peaks obtained from SCG cultures

Observed mass	Observed ions in MS^2	Observed ions in MS^3	Assigned molecular species
m/z	*m/z*	*m/z*	
848	789	665	[PC(diacyl-18:0/20:4)+K]$^+$
844	785	661	[PC(diacyl-16:0/22:6)+K]$^+$
846	787	663	[PC(diacyl-18:1/20:4)+K]$^+$
872	813	689	[PC(diacyl-18:0/22:6)+K]$^+$
826	767	643	[PC(diacyl-18:0/18:1)+K]$^+$
772	713	589	[PC(diacyl-16:0/16:0)+K]$^+$
798	739	615	[PC(diacyl-16:0/18:1)+K]$^+$
824	765	641	[PC(diacyl-18:0/18:2)+K]$^+$

position of PC molecular species was quantified by LC-ESI-MS/MS, which provides precise quantitative information (18). The observed signal "spots" in the maps (Fig. 2*A*) represent distinct molecular species of PC and sphingomyelin lipid classes; a precursor ion scan of *m/z* 184, used as an MS/MS method in the present study, specifically detected ions that contained a trimethylamine group in their structure, *i.e.* a head group of PC and sphingomyelin (19). Interestingly, we found that the intensity of PC(diacyl-18:0/20:4), *i.e.* AA-PC, was highest among the long chain polyunsaturated fatty acid (LCPUFA)-PCs, which contain four or six double bonds at their *sn*-2 positions. LCPUFA-PCs (shown in *red* or *black letters* in Fig. 2) were detected at higher levels in the axon than in the cell body, whereas PCs containing saturated fatty acid (SA; 16:0 or 18:0), monounsaturated fatty acid (MUSA; 18:1), or linoleic acid (LA; 18:2) at their *sn*-2 position (shown in *gray letters* in Fig. 2) were detected at lower levels in the axon than in the cell body or at similar levels in both regions.

To determine whether the MALDI-based measurements reflect the quantitative results of LC-ESI-MS/MS, we measured the SCG culture with MALDI-MS (Fig. 2*B*). Consistent with the LC-ESI-MS/MS results, the signal intensity of AA-PC(18:0/20:4) was higher in the axon than in the cell body/juxta. The overall quantification results from MALDI-MS are shown in Fig. 2*C*. At the cell body/juxta and axon, MUSA-PCs (*i.e.* 18:0/18:1 and 16:0/18:1) accounted for approximately half of the total PC population, whereas SA-PCs (16:0/16:0 and 16:0/18:0) accounted for approximately one quarter. Interestingly, LCPUFA-PCs (*dark gray field*) accounted for a higher percentage at the axon than at the cell body/juxta, whereas LA-PCs (*light gray field*) accounted for a higher percentage at the cell body/juxta than at the axon. In particular, AA-PC accounted for the highest percentage among LCPUFA-PCs at the cell body/juxta as well as the axon. Moreover, AA-PC showed higher localization at the axon than at the cell body/juxta. Our data demonstrate that compared with SA/MUSA/LA-PCs, AA-PC is highly localized in the axon rather than in the cell body.

Increasing Intensity of AA-PC along Proximodistal Axis of Axon—Having demonstrated higher localization of AA-PC in the axon than in the cell body, we investigated whether AA-PC is distributed heterogeneously along the axon and, if so, where it localizes. MALDI-imaging clearly demonstrated the heterogeneous distribution of PC species within the axon (Fig. 3*A*). The most conspicuous feature of this PC distribution was an exponential-like increase of AA-PC along the proximodistal axis of the axon (Fig. 3*A*, *left*). Therefore, it could be said that AA-PC tends to localize in the distal part of the axon. In contrast, SA/MUSA/LA-PCs showed decreasing or almost flat distributions along the axonal length (Fig. 3*A*, *middle* and *right*). Because AA-PC showed an exponential-like increase, we performed a logarithmic transformation of the intensity and found a linear correlation between the log AA-PC signal intensity and distance from the cell body (Fig. 3*B*, *left*).

To confirm the reproducibility of this finding in several cells, we assessed the linear relationship between PC intensity and axonal distance by the image analyses described under "Experimental Procedures." We validated the linearity of the AA-PC plot for intensity (*vertical axis*) and axonal distance (*horizontal axis*) (Fig. 3*C*, *left*, $R^2 = 0.9$). This linearity enabled us to calculate and utilize an axonal slope coefficient index, namely "*k*", as a simple representative for the axonal PC distribution pattern relative to the distance from the cell body; *k* is positive when PC intensity is increasing along the axon (Fig. 3*C*, *left*), almost zero when the PC intensity does not exhibit a specific tendency along the axon (Fig. 3*C*, *middle*), and negative when the PC intensity is decreasing along the axon (Fig. 3*C*, *right*). The distributions of the 10 major PC molecular species are summarized in Fig. 3*D*. In particular, the intensity of AA-PC was higher at the distal axon than the proximal axon. Moreover, AA-PC showed the highest *k* value among the major PCs. In contrast, SA/MUSA/LA-PCs (of negative or near zero *k* values) showed a reduction or no specific changes in their intensity from the proximal to the distal axon (Fig. 3*D*).

Quantitative analyses of metabolites by MS can be performed by LC-ESI-MS/MS with the use of multiple reaction monitoring (18). To validate the PC distribution pattern, we introduced LC-ESI-MS/MS with multiple reaction monitoring and performed quantitative analyses of PC species between the proxi-

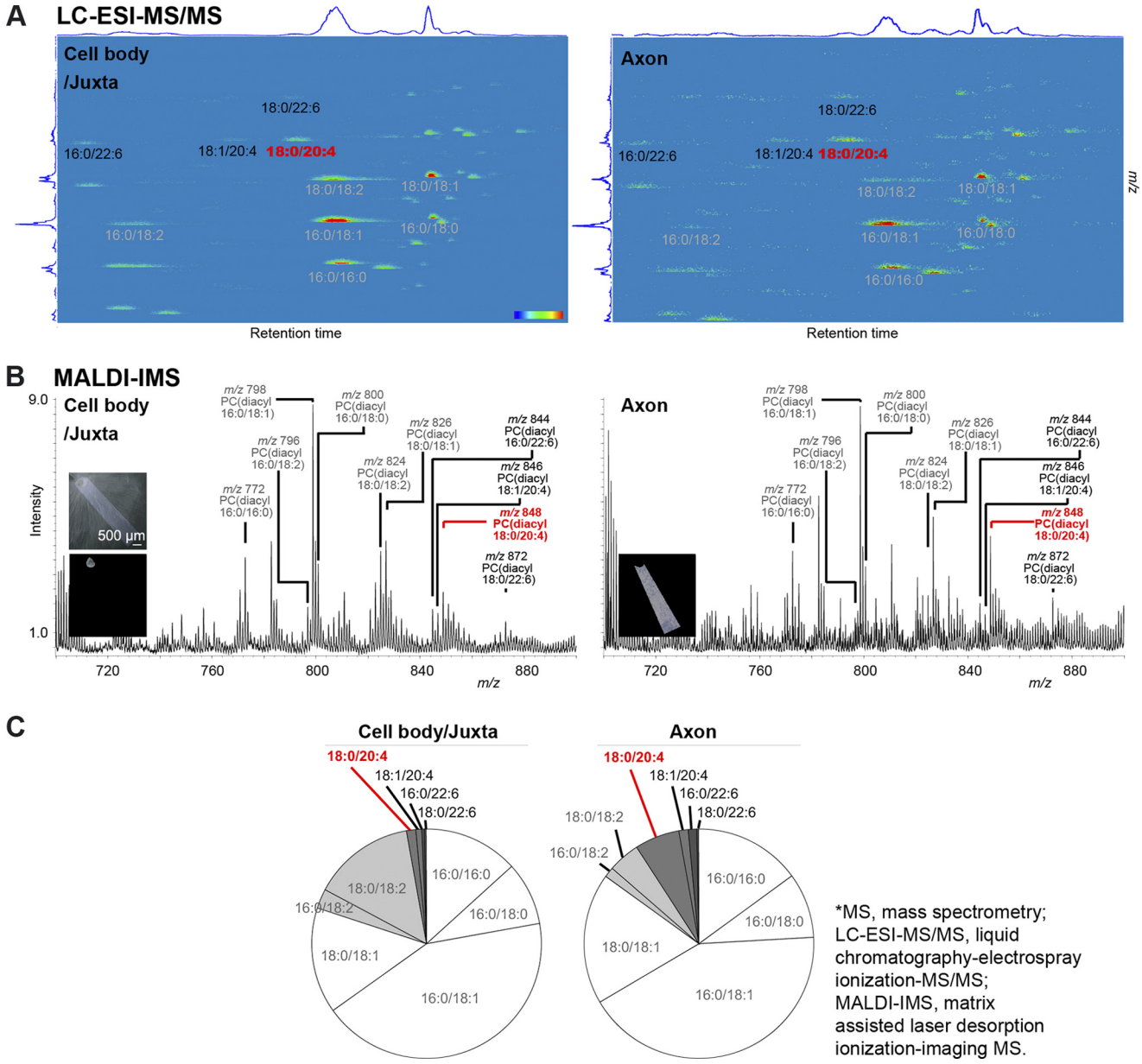

FIGURE 2. **Intensity of AA-PC in the axon and cell body.** Signals (*A* and *B*) or percentage (*C*) of major PC species in the cell body/juxta (*left*) and axon (*right*) are shown. *Gray letters* indicate PCs containing SA, MUSA, or LA, whereas *red* and *black letters* indicate AA-PC and PCs containing LCPUFA except AA-PC, respectively. Each experiment was repeated at least three times, and representative data are shown. *A*, LC-ESI-MS/MS analysis. Detected ions are shown against the retention time resolved by LC (*horizontal axis*) and the *m/z* value resolved by MS (*vertical axis*). The *color scale bar* represents signal intensity, with *red* indicating the greatest intensity and *blue* representing the lowest intensity. *B*, mass spectrum from MALDI-MS. *Left upper inset* is a picture of the measured region. *Left lower* and *right lower insets* are total ion images of the cell body/juxta and axon, respectively. *Scale bar*, 500 μm. *C*, graphs of MALDI-MS analysis of PC compositions in the cell body/juxta and axon. The percentage of each PC species is indicated by the following colors: SA/MUSA-PCs (*white*), LA-PCs (*light gray*), AA-PCs (*gray*), DHA-PCs (*dark gray*).

mal and distal axon. There was a slight reduction in the total amount of major PC species at the distal axon, which derived from the reduction of axonal numbers (data not shown). Thus, to compare PC amounts per axon, we normalized to the sum of major PC species; intriguingly, the relative amount was consistent with the MALDI-MS data. For example, we present the cases of AA-PC and LA-PC(diacyl-16:0/18:2), which showed the highest and lowest *k* values (Fig. 3*D*). This result validated the higher distribution of AA-PC and lower distribution of LA-PC at the distal axon compared with the proximal axon (Fig. 3*E*). The LC-ESI-MS/MS data suggested that the amount of AA-PC gradually increased as it progresses from the cell body at the single axon level. Taken together, our results indicate that AA-PC was heterogeneously distributed, with increasing intensity, along the axon.

Localization of AA-PC in Distal Axon in Early Stage Culture—To determine when the distribution of AA-PC along the axon is initiated, we prepared SCG cultures of DIV 1 to DIV 5 and used MALDI-imaging to assess the axonal PC distribution. We found that the gradient of AA-PC along the axon was present at DIV 1, although the axonal length was much shorter than it was at DIV 5. This pattern was observed from DIV 1 to DIV 5 (Fig. 4*A*, *left*). During the same period, PC(diacyl-16:0/18:0) consistently showed an almost flat distribution pattern (Fig. 4*A*, *mid-*

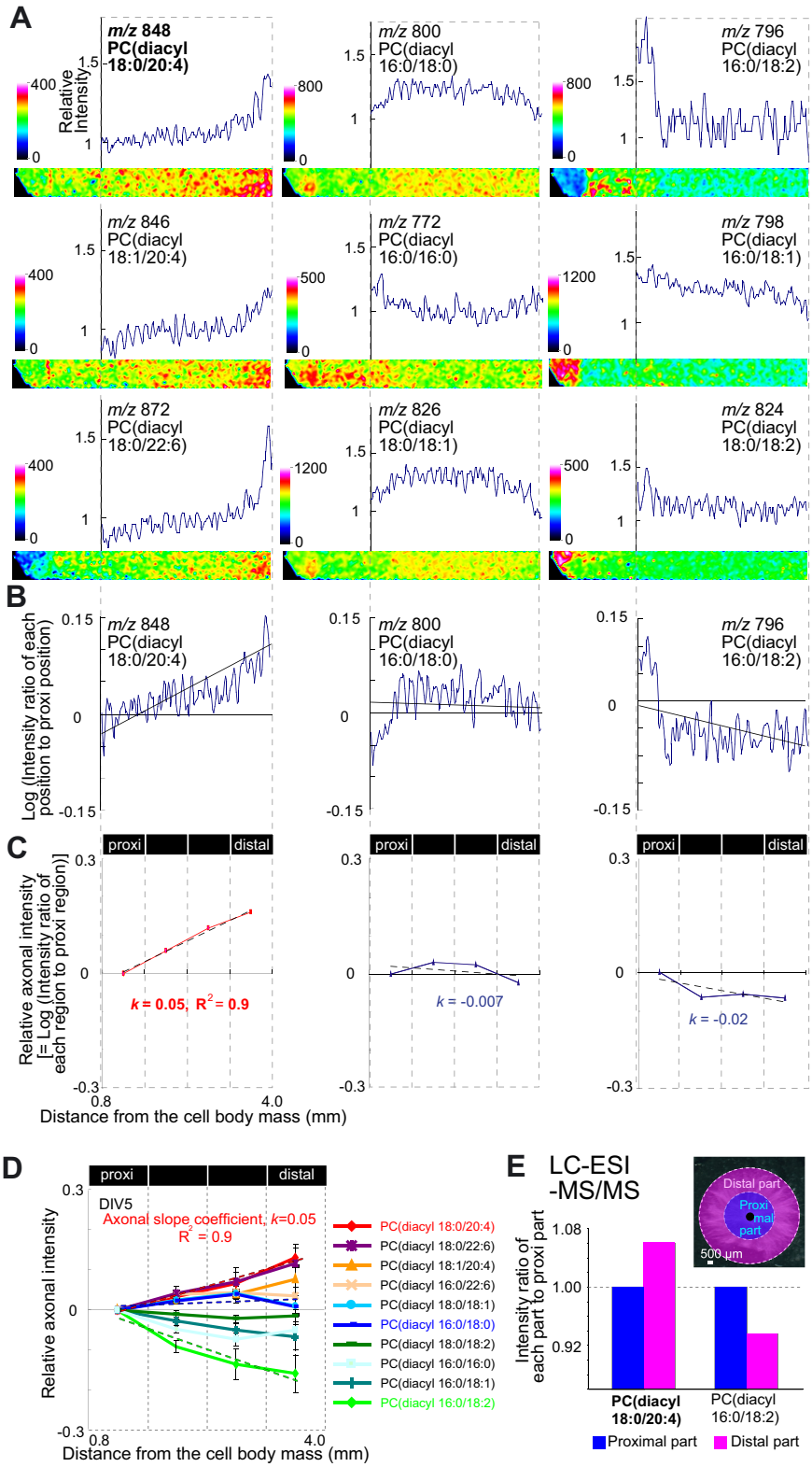

FIGURE 3. **Gradual increase in AA-PC intensity along the axon.** Each experiment was performed at least three times, and representative data are shown. *A*, representative ion distribution images and intensity graphs of major PC species. Briefly, SCG neurons were freeze-dried, sprayed with matrix, and immediately used for MALDI-imaging. In each image, the *left side* contains the cell body mass, and the *right side* corresponds to the distal axon. To obtain the graph, the averaged intensity of each row of pixels was numerically converted by Scion image (Scion, Frederick, MD). Each graph shows relative intensity (*vertical axis*) *versus* distance from the cell body (*horizontal axis*). The relative intensity is presented in *color*, with high and low intensity corresponding to *white* and *black* in the *color bar*. *B*, linear relationship between the log of the intensity ratio of each region to proximal (*proxi*) region (*vertical axis*) and distance (*horizontal axis*). *C*, image analyses of axonal intensity. Based on the linear relationship between AA-PC axonal intensity and distance, we derived the axonal slope, *k*, by dividing the indicated axonal region into four parts. *D*, graphs of axonal intensity and distance for major PCs. Three different explant cultures at DIV 5 were used for analyses. *E*, LC-ESI-MS/MS analysis of extracted PC from the proximal and distal parts of the axon. Axons were divided into two parts (*inset*) and were separately collected and used for LC-ESI-MS/MS. Six explant cultures were pooled for the measurement.

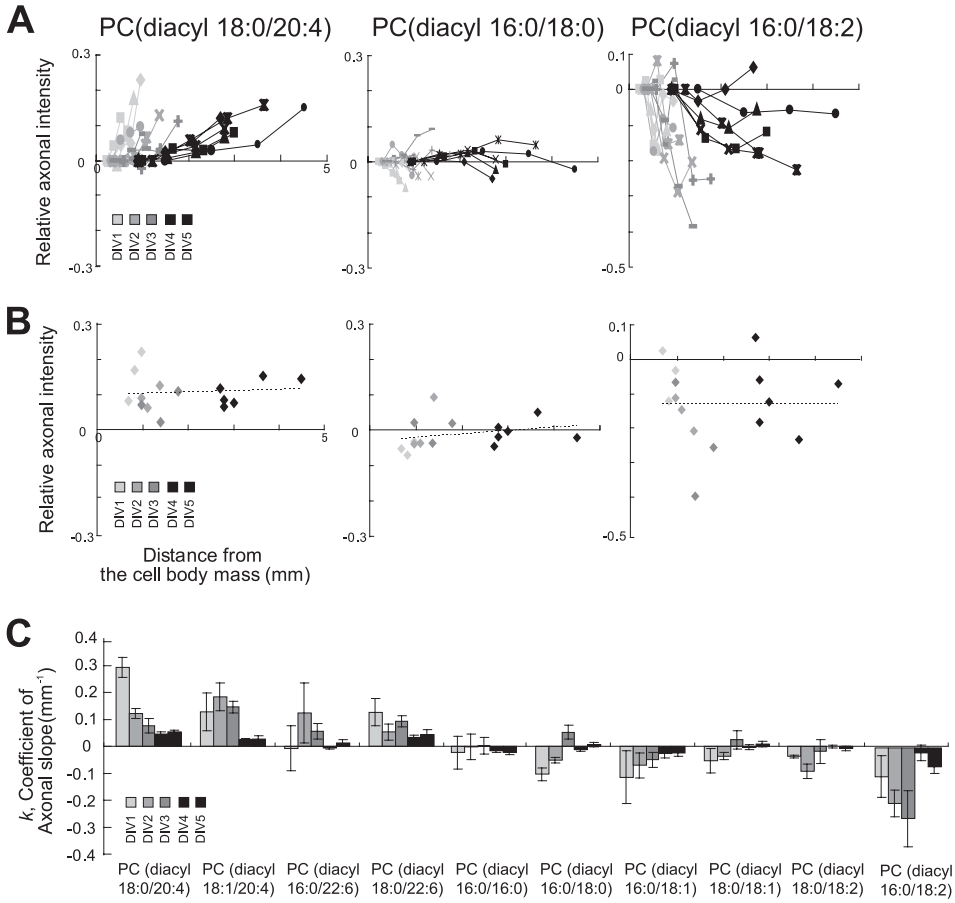

FIGURE 4. **High intensity of AA-PC in the distal axon was observed from DIV 1 and maintained until DIV 5.** *A*, relative axonal intensities (*vertical axis*) of the three representative PC species *versus* the distance (*horizontal axis*) from the cell body mass. *Line colors* represent culture days: *light gray*, *gray*, *dark gray*, *dense dark gray*, and *black* represent DIV 1, DIV 2, DIV 3, DIV 4, and DIV 5, respectively. The three different explant cultures are represented by different *dot styles*. *B*, axonal intensities of PCs at the distal axon are plotted *versus* distance from the cell body mass. The *proximate line* shows that the distal axon intensities of PCs were maintained throughout the culture period. *C*, *k* values for the 10 major PC species during DIVs 1–5. The axonal slope of each DIV was calculated from three different explant cultures.

dle). The decreasing distribution of PC(diacyl-16:0/18:2) was consistently observed in growing cultures (Fig. 4*A*, *right*). These consistent distribution patterns throughout the culture period (Fig. 4*B*) indicate that the major PC composition of proximal and distal axons is determined during early stage culture and maintained during axonal growth, at least in the culture system used here.

Analyses of the *k* value from DIV 1 to DIV 5 indicated a gradual reduction in AA-PC axonal slope (Fig. 4*C*, *left*). This may suggest that the high abundance of AA-PC at the distal part of the axon was relatively stable. Therefore, increasing axonal length resulted in a gradually decreasing slope. The *k* values of SA/MUSA/LA-PCs were negative or near zero (−0.3 to 0.05; Fig. 4*C*, *right*, six PCs), indicating that the intensities of SA/MUSA/LA-PCs showed consistently flattening or decreasing patterns along the axonal length. These results demonstrate that the increasing axonal intensity of AA-PC occurred from the early stage of culture (*i.e.* at DIV 1) and was maintained throughout the culture period.

Inhibition of Actin Dynamics Reduces Axonal Gradient of AA-PC—It is well known that cytoskeletal structures modulate the movement of intracellular membranes. The dynamics of the actin cytoskeleton can become a driving force that mobilizes intracellular components (7), influencing the redistribution of membrane compartments. We investigated whether actin dynamics play a role in the distribution of AA-PC. We treated neurons with cytochalasin D, which inhibits the association and dissociation of globular (G)-actin by binding to the barbed end of filamentous (F)-actin (20). Cytochalasin D yielded normal staining of α-tubulin but weak staining of F-actin (Fig. 5*A*, *left*), suggesting an actin-specific disruption. We confirmed that cytochalasin D did not affect cell viability by observing that cytochalasin D-treated neurons were calcein AM-positive (Fig. 5*A*, *right*). We treated SCG neurons with vehicle or cytochalasin D for 2 h and analyzed the results using MALDI-imaging (Fig. 5*B*). Intriguingly, we found that cytochalasin D reduced the signal intensity of AA-PC, particularly in the distal part of the axon, compared with the vehicle control (Fig. 5*B*, *left*). Moreover, the *k* for AA-PC was significantly reduced following cytochalasin D treatment ($k = 0.05 \pm 0.002$, average ± S.E.) compared with the vehicle control ($k = 0.1 \pm 0.001$, Fig. 5*C*).

To investigate further the effect of actin dynamics on AA-PC axonal distribution, we used phallacidin, a cell-permeable analog of phalloidin that inhibits F-actin transition to G-actin by preventing depolymerization (21), with negligible cytotoxicity

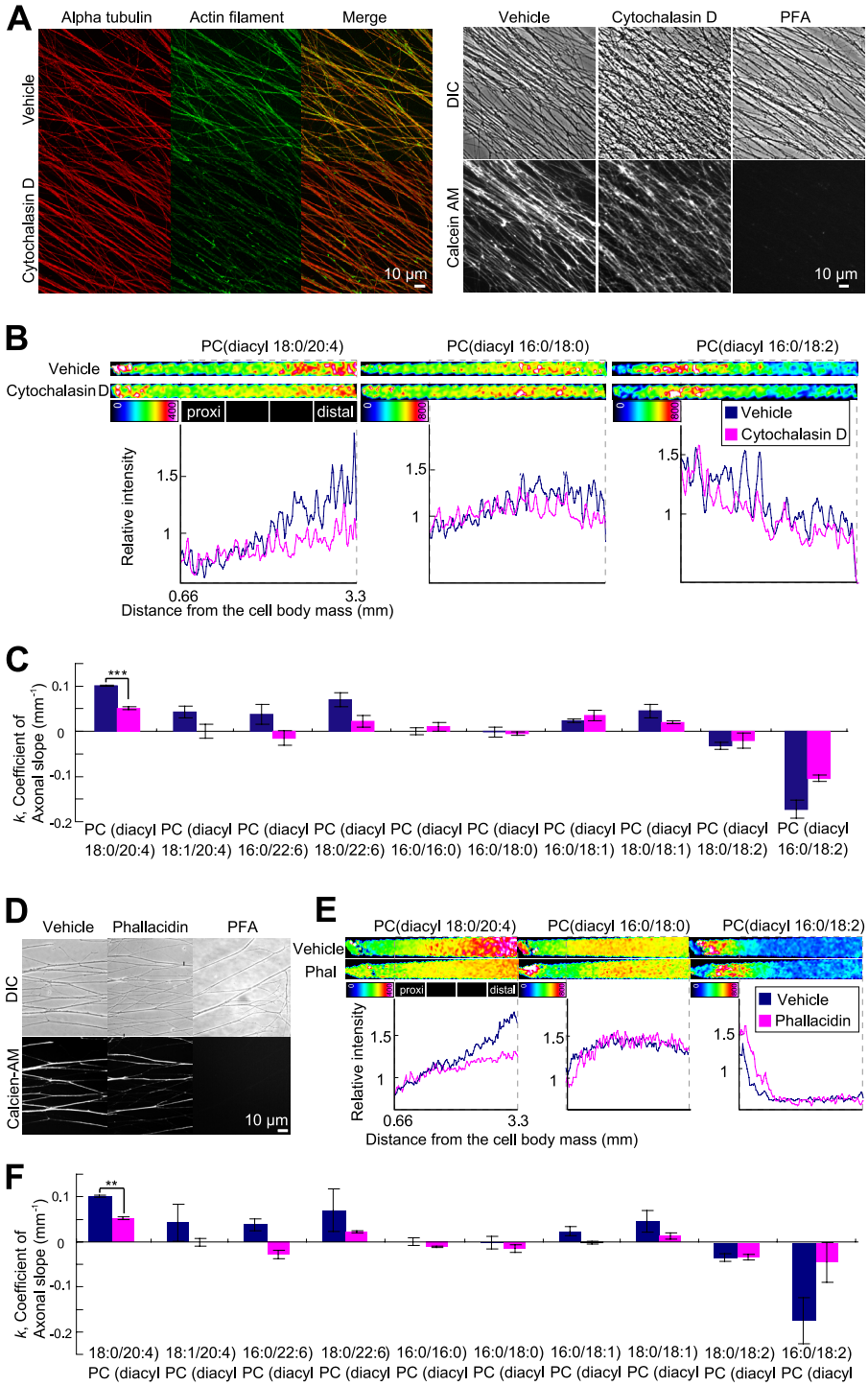

FIGURE 5. **Inhibition of actin dynamics reduced axonal intensity of AA-PC in distal axon.** *A*, *left*, immunostaining of α-tubulin and F-actin in neurons treated with 40 μg/ml cytochalasin D and its vehicle. *Right*, calcein-AM staining in neurons treated with the indicated reagents. *Scale bars*, 10 μm. *B* and *C*, *blue* and *red colors* representing the intensity or coefficient from vehicle- and cytochalasin D-treated neurons, respectively. *B*, representative ion images of three PC species in neurons treated with vehicle and cytochalasin D. Graphs of relative intensity (*vertical axis*) *versus* distance (*horizontal axis*) are shown. *C*, axonal slope coefficients for major PC species in vehicle and cytochalasin D-treated neurons. AA-PC(diacyl-18:0/20:4) showed a significant reduction in *k* value (Student's *t* test, ***, $p < 0.001$, $n = 3$). *Error bars*, S.E. *D*, calcein-AM staining in neurons treated with the indicated reagents. *Scale bar*, 10 μm. *E* and *F*, *blue* and *red* representing the intensity or coefficient from vehicle- and phallacidin-treated neurons, respectively. *E*, ion distribution images of three representative PC species in neurons treated with 25 μM phallacidin and its vehicle. Graphs of relative intensity (*vertical axis*) *versus* distance (*horizontal axis*) are shown. *F*, axonal slope coefficients for major PC species in vehicle- and phallacidin-treated neurons. AA-PC(diacyl-18:0/20:4) showed a significant reduction in *k* value (Student's *t* test, **, $p < 0.01$, $n = 3$). Each experiment was performed at least three times.

(22). We first confirmed that phallacidin treatment did not affect cell viability (Fig. 5*D*) and then performed MALDI-imaging. Intriguingly, the distribution of AA-PC in the phallacidin-treated neurons showed a dramatic reduction in axonal intensity (Fig. 5*E*), consistent with the results of cytochalasin D treatment. Moreover, the *k* value for AA-PC was significantly

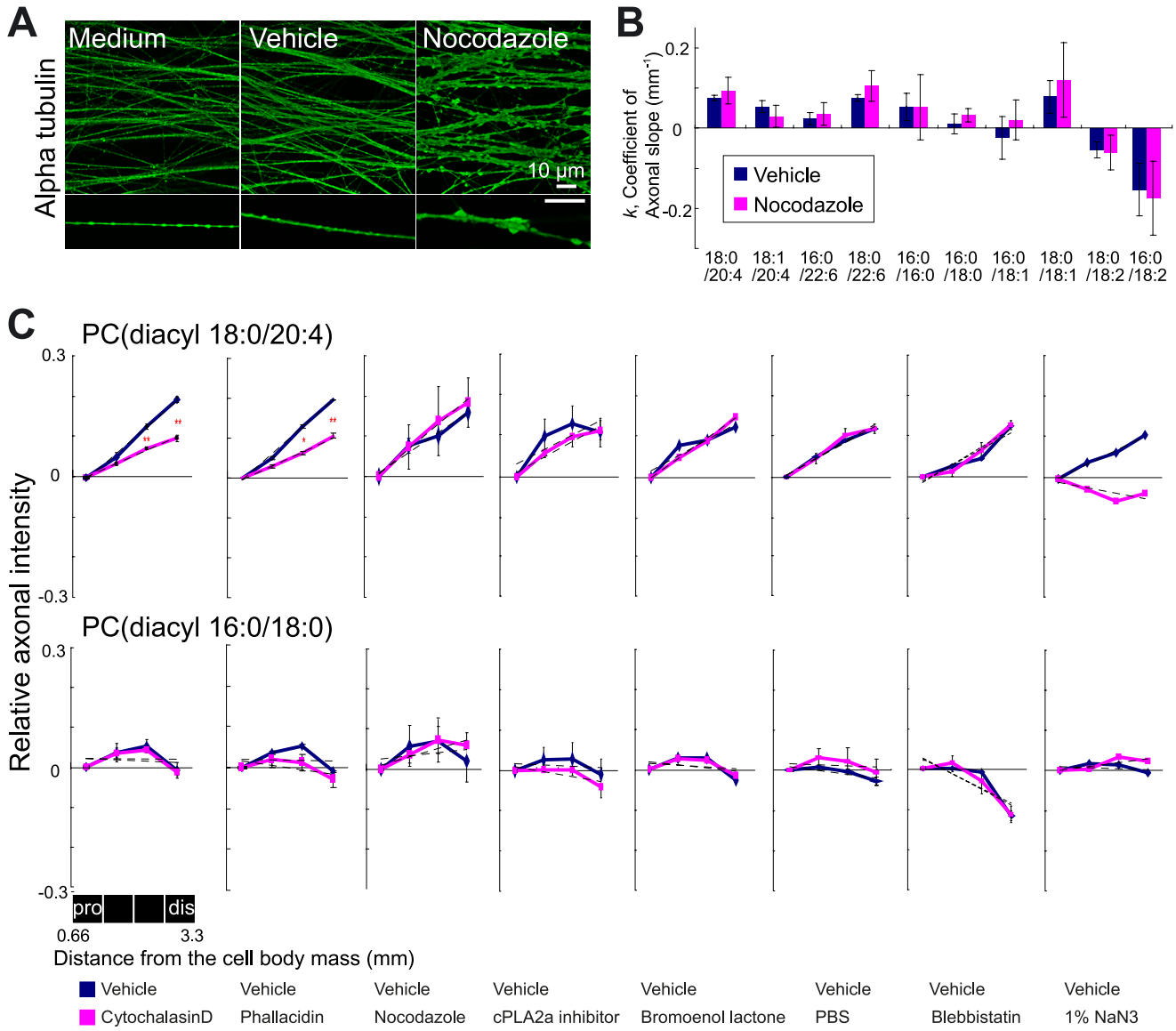

FIGURE 6. **Inhibitor treatment for other possible factors that may affect the axonal slope did not change the axonal slope of AA-PC.** *A*, immunostaining of α-tubulin in neurons treated with medium, vehicle, and nocodazole (10 μg/ml). *Scale bar*, 10 μm. *B*, *blue* and *red colors* representing the coefficient *k* from vehicle- and nocodazole-treated neurons, respectively. Three different explant cultures were used for each treatment. *C*, summary of inhibitor treatments. *Upper*, changes in relative axonal intensity of AA-PC by inhibitor treatment. Treatments for actin dynamic inhibitors, *i.e.* cytochalasin D (Student's *t* test, ** $p < 0.01$, $n = 3$) and phallacidin (Student's *t* test, * $p < 0.05$, ** $p < 0.01$, $n = 3$) decreased the slope, as did sodium azide. *Lower*, changes in relative axonal intensity of SA-PC. Each experiment was performed at least twice.

reduced following phallacidin treatment ($k = 0.05 \pm 0.003$) compared with the vehicle control ($k = 0.1 \pm 0.002$, Fig. 5*F*). The consistency between the results of phallacidin and cytochalasin D treatments indicates that the observed axonal slope reduction of AA-PC is caused by inhibition of actin dynamics.

Effects of Other Inhibitors on Axonal Distribution of AA-PC—Having demonstrated that inhibition of actin dynamics significantly influences axonal localization of AA-PC, we investigated whether the disruption of another major cytoskeleton, *i.e.* microtubule, has a similar effect (Fig. 6*A*, B). We used nocodazole, which disrupts microtubules, inducing axonal swelling (Fig. 6*A*). However, it did not produce significant changes in the axonal slope for AA-PC (Fig. 6*B*), indicating that the axonal slope of AA-PC is not significantly contributed by microtubule. The significant changes of AA-PC axonal slope in neurons treated with actin inhibitors raise a possibility that a myosin motor walking on actin contributes to the distribution. However, this possibility was also dismissed by myosin motor blockage using blebbistatin; AA-PC axonal slope was not changed after blebbistatin treatment (Fig. 6*C*).

To understand the formation of AA-PC axonal slope, we treated neurons with several inhibitors that block specific pathways of AA-PC metabolism. Once PC is synthesized, it enters into a remodeling pathway in which phospholipase plays roles to make LCPUFA-PCs. Phospholipase might affect on axonal distribution of AA-PC. To check this hypothesis, we treated cells with cPLA2α inhibitor or calcium-independent phospholipase (iPLA) 2 inhibitor (bromoenol lactone) (23). However,

they did not induce significant changes in the distribution of AA-PC on axon (Fig. 6*C*), suggesting that AA-PC axonal distribution is not significantly correlated with the phospholipase activity. The axonal gradient of AA-PC might be also derived from different intake ratio of the medium depending on the axon region. To investigate this, we replaced the culture medium with PBS and measured AA-PC axonal intensity. This hypothesis was also discarded because of no significant changes on AA-PC axonal intensity by PBS replacement.

To confirm whether the AA-PC axonal slope is derived from healthy neurons and not from dead ones, we treated neurons with sodium azide and compared them with normal neurons. The results showed that the AA-PC axonal slope was not present in neurons treated with sodium azide, indicating that AA-PC localization is ATP-dependent and not present in dead cells. Throughout the experiments, PC(diacyl-16:0/18:0) consistently showed *k* values that were near zero, indicating no significant changes between the vehicle and the indicated reagent (Fig. 6*C*, *lower*). In summary, the increasing axonal intensity of AA-PC along the axon was specifically influenced by inhibition of actin dynamics, but not by disruption of myosin, microtubules, PC metabolism, or medium depletion.

DISCUSSION

AA mediates neuronal function (2, 4) and has been implicated in neurodegenerative diseases (24). AA is rapidly incorporated into PC (25), suggesting rapid reacylation. Although the crucial neuronal function of AA has been suggested, the distribution of AA-PC has not been reported at the intracellular level. We characterized the distribution of AA-PC inside the neuron and found an increasing gradient of AA-PC along the proximodistal axonal axis. Further, our results indicated that these gradients depend on actin dynamics.

Possible Biological Function of Axonal Gradient of AA-PC—AA-PC(diacyl-38:4) is a major PC species in SCG neurons, and its acyl chains were assigned as PC(diacyl-18:0/20:4) (Table 1) based on evidence indicating that endogenous PC possesses PUFAs at *sn*-2 positions rather than at *sn*-1 positions (18). MALDI-imaging MS and LC-ESI-MS/MS data showed that AA-PC is more highly localized at the axon rather than at the cell body (Fig. 2). Inside the axon, the intensity of AA-PC gradually increased toward the distal axon (Fig. 3). This gradient was also observed for docosahexaenoic acid (DHA)-PC, but not SA/MUSA/LA-PCs. According to magnetic resonance spectroscopy, there are structural differences between LCPUFA-PCs (*i.e.* AA-PC and DHA-PC) and SA/MUSA/LA-PCs (26). LCPUFA-PCs have a larger volume at *sn*-2 and shorter length at *sn*-1 than SA/MUSA/LA-PCs do, indicating a lower PC density on membranes containing LCPUFA-PCs *versus* a higher density on membranes containing SA/MUSA/LA-PCs. Thus, the distal axon, which contains more LCPUFA-PCs, may be more flexible than the proximal axon, which contains more SA/MUSA/LA-PCs. This idea is consistent with the previous report that the axon membrane exhibits a gradient from a lower membrane tension at the growth cone to a higher membrane tension at the cell body (27). Further, high localization of LCPUFAs, which can be released from LCPUFA-PCs, on the distal axon might affect membrane protein function by changing bilayer elasticity (28).

Another possible biological function of the axonal gradient of AA-PC is the timely source for AA release. The release of free AA can be initiated by activation of various receptors followed by enzyme-mediated hydrolysis of membrane phospholipids. AA-PC can be effectively hydrolyzed by PLA2, releasing free AA (29). Released AA has several possible functions, including modulation of voltage-gated ion channels as well as protein kinases and signal transduction cascades, and thus modulates neuronal excitability (30). As AA mediates intracellular signaling cascades, it is crucial to keep the concentration of free AA low within cells. Thus, the higher concentration of AA-PC near the axon terminal might provide a timely source of free AA, rapidly providing them only during the activated period.

Possible Mechanism of Maintaining Axonal Gradient of AA-PC—PC is synthesized by *de novo* synthesis and maintained by a remodeling pathway. Because it is a major membrane component, it may be transported to various locations inside the cell. Thus, the distribution of AA-PC is controlled by *de novo* synthesis, remodeling, and transport.

De Novo Synthesis—To determine the likelihood of *de novo* synthesis, we replaced the medium with PBS, thus shutting down the external source of AA (Fig. 6*C*). Neurons lack the desaturase and elongase enzymes needed to synthesize AA or DHA from their fatty acid precursors; thus, they require PUFAs to be provided from the outside environment (31). Long chain fatty acids can be passively taken up by cells by diffusion through membrane lipids. Membrane components that facilitate uptake of long chain fatty acids along the axon can contribute to formation of the axonal gradient of AA-PC. However, this possibility was dismissed because of the unaltered gradient of AA-PC when the medium was replaced with PBS (Fig. 6*C*). This indicates no requirement for exogenous AA to maintain the axonal gradient of AA-PC during the tested incubation time. We used a 2-h incubation period for medium replacement and other inhibitors. This period was sufficient to induce observable changes in AA-PC, based on the reported PC half-life. In the brain of pentobarbital-anesthetized rats, the half-life of PCs containing AA, such as PC(16:0/20:4) or PC(18:0/20:4), is ~2–3 h (32). A similar half-life was observed for PC precursors in PC12 cells: choline for 58 min and phosphorylcholine for 90 min (33).

Remodeling Pathway—Another possible explanation for the axonal AA-PC gradient is that it is the product of the distribution or activity of the enzymes involved in AA-PC metabolism; however, there has been no report on the axonal distribution of enzymes involved in AA-PC metabolism. After *de novo* PC synthesis, the fatty acyl composition at the *sn*-2 position is altered by the remodeling pathway via reacylation (5) or deacylation enzymes (34). For reacylation, LPCAT2 and -3 have preferences for AA, but only LPCAT3 results in diacyl-PC (5), to which AA-PC belongs. Considering that the expression of LPCAT 3 in the brain is very low compared with other tissue types (35), the AA-PC remodeling pathway in neurons might be regulated mainly by activation or deactivation of PLA2, although there may also be an unknown LPCAT. In the mammalian system,

deacylation is mediated by more than 19 different isoforms of PLA2, which cleaves fatty acids from the *sn*-2 position of phospholipids. They can be divided into three major groups: cPLA2, iPLA2, and secretory PLA2 (36). cPLA2 exhibits high selectivity for AA at the *sn*-2 position of the glycerol backbone (37), and iPLA2 is considered a major source for the release of DHA (23) but is also reported as a source for AA (38). PLA2 activities were observed in SCG, and some of them depend on Ca^{2+}, but others remain active in the absence of Ca^{2+}, indicating that both cPLA2 and iPLA2 exist in SCG (39). Although PLA2 activities exist in SCG, the possibility of their contribution to the axonal gradient of AA-PC was dismissed by the unaltered axonal gradient of AA-PC after treatment of cells with inhibitors of cPLA2 or iPLA2 (Fig. 6). We did not test soluble PLA2 because its mRNA is not constitutively expressed; it only is induced by certain conditions in the peripheral nervous system and has no fatty acid preference (40), so it does not specifically affect the metabolism of AA-PC. Thus, it seems that reacylation/deacylation is not the main contributor to the AA-PC axonal gradient in our culture system.

Microtubule Transport—Another mechanism that may drive the axonal gradient of AA-PC is microtubule or actin transport. Microtubules are the major longitudinal cytoskeletal filament in axons. Kinesins and dyneins move along microtubules in vesicle transport (41). If the enzymes that mediate AA-PC or its metabolism are transported on microtubules, the axonal gradient of AA-PC would be altered by inhibition of microtubule transport. However, the gradient was unchanged by nocodazole treatment (Fig. 6), indicating that the axonal gradient of AA-PC is not derived from microtubule-dependent transport.

Transport by Actin via Myosin—Actin transport can be mediated by myosin walking along an actin filament or by actin dynamics. The former hypothesis was dismissed by the unaltered axonal gradient of AA-PC on neurons treated with blebbistatin, a cell-permeable inhibitor of ATPase activity of the A and B isoforms of non-muscle myosin II (42) (Fig. 6*C*). Although there are other types of myosin such as class I, V, and VI, myosin II is suggested to be the most crucial at the growth cone (43).

Transport by Actin Dynamics—Finally, we found out that the axonal gradient of AA-PC was decreased significantly by inhibition of actin filament polarization and depolarization (Fig. 5). Thus, it seems that actin dynamics maintain the axonal gradient of AA-PC. Although it is remained to be investigated how the inhibition of actin dynamics changed the axonal gradient of AA-PC, we can speculate on its mechanism; actin dynamics may restrict the distribution of AA-PC because actin polymerization (7, 44) and depolymerization (45, 46) could affect the intracellular motility of vesicles containing AA-PC. The turnover of actin filaments is an energy-consuming process that requires ATP. Thus, we also tested sodium azide, which inhibits ATP synthesis (47). Sodium azide treatment reduced the axonal gradient of AA-PC (Fig. 6), indicating that ATP is required for maintaining the gradient.

In our previous study, AA-PC was localized more to the hippocampal area than to other parts of the rodent brain (10). This study revealed that the polarity of AA-PC distribution exists within the cells. Our elucidation of the actin-related distribution of AA-PC inside neurons reveals a new aspect of PC localization and regulation in neurons.

Acknowledgments—We thank Professor Elior Peles of the Weizmann Institute for helpful comments on the manuscript and Shimadzu Corporation for the Analysis software used in the imaging mass spectrometry experiments. We are grateful to Professor Sano of the University of Tokyo and Professor Tazaki of the University of Gakushuin for discussions concerning mathematical calculations and Professor Watanabe of the University of Tohoku for helpful discussions concerning actin dynamics.

REFERENCES

1. Sanchez-Mejia, R. O., Newman, J. W., Toh, S., Yu, G. Q., Zhou, Y., Halabisky, B., Cissé, M., Scearce-Levie, K., Cheng, I. H., Gan, L., Palop, J. J., Bonventre, J. V., and Mucke, L. (2008) Phospholipase A2 reduction ameliorates cognitive deficits in a mouse model of Alzheimer's disease. *Nat. Neurosci.* **11,** 1311–1318
2. Nomura, T., Nishizaki, T., Enomoto, T., and Itoh, H. (2001) A long lasting facilitation of hippocampal neurotransmission via a phospholipase A2 signaling pathway. *Life Sci.* **68,** 2885–2891
3. Vijayaraghavan, S., Huang, B., Blumenthal, E. M., and Berg, D. K. (1995) Arachidonic acid as a possible negative feedback inhibitor of nicotinic acetylcholine receptors on neurons. *J. Neurosci.* **15,** 3679–3687
4. Williams, J. H., Errington, M. L., Lynch, M. A., and Bliss, T. V. (1989) Arachidonic acid induces a long term activity-dependent enhancement of synaptic transmission in the hippocampus. *Nature* **341,** 739–742
5. Shindou, H., and Shimizu, T. (2009) Acyl-CoA:lysophospholipid acyltransferases. *J. Biol. Chem.* **284,** 1–5
6. Takamori, S., Holt, M., Stenius, K., Lemke, E. A., Grønborg, M., Riedel, D., Urlaub, H., Schenck, S., Brügger, B., Ringler, P., Müller, S. A., Rammner, B., Gräter, F., Hub, J. S., De Groot, B. L., Mieskes, G., Moriyama, Y., Klingauf, J., Grubmüller, H., Heuser, J., Wieland, F., and Jahn, R. (2006) Molecular anatomy of a trafficking organelle. *Cell* **127,** 831–846
7. Merrifield, C. J., Moss, S. E., Ballestrem, C., Imhof, B. A., Giese, G., Wunderlich, I., and Almers, W. (1999) Endocytic vesicles move at the tips of actin tails in cultured mast cells. *Nat. Cell Biol.* **1,** 72–74
8. Lang, T., Wacker, I., Wunderlich, I., Rohrbach, A., Giese, G., Soldati, T., and Almers, W. (2000) Role of actin cortex in the subplasmalemmal transport of secretory granules in PC-12 cells. *Biophys. J.* **78,** 2863–2877
9. Small, J. V., and Resch, G. P. (2005) The comings and goings of actin: coupling protrusion and retraction in cell motility. *Curr. Opin. Cell Biol.* **17,** 517–523
10. Sugiura, Y., Konishi, Y., Zaima, N., Kajihara, S., Nakanishi, H., Taguchi, R., and Setou, M. (2009) Visualization of the cell-selective distribution of PUFA-containing phosphatidylcholines in mouse brain by imaging mass spectrometry. *J. Lipid Res.* **50,** 1776–1788
11. Rubakhin, S. S., Churchill, J. D., Greenough, W. T., and Sweedler, J. V. (2006) Profiling signaling peptides in single mammalian cells using mass spectrometry. *Anal. Chem.* **78,** 7267–7272
12. Rubakhin, S. S., and Sweedler, J. V. (2007) Characterizing peptides in individual mammalian cells using mass spectrometry. *Nat. Protoc.* **2,** 1987–1997
13. Ostrowski, S. G., Van Bell, C. T., Winograd, N., and Ewing, A. G. (2004) Mass spectrometric imaging of highly curved membranes during *Tetrahymena* mating. *Science* **305,** 71–73
14. Sjövall, P., Lausmaa, J., Nygren, H., Carlsson, L., and Malmberg, P. (2003) Imaging of membrane lipids in single cells by imprint-imaging time-of-flight secondary ion mass spectrometry. *Anal. Chem.* **75,** 3429–3434
15. Ikegami, K., and Koike, T. (2003) Non-apoptotic neurite degeneration in apoptotic neuronal death: pivotal role of mitochondrial function in neurites. *Neuroscience* **122,** 617–626
16. Yang, H. J., Sugiura, Y., Ishizaki, I., Sanada, N., Ikegami, K., Zaima, N., Shrivas, K., Setou, M., and (2010) Imaging of lipids in cultured mammalian

neurons by matrix assisted laser/desorption ionization and secondary ion mass spectrometry. *Surf. Interface Anal.* **42,** 1606–1611
17. Moore, M. W., Klein, R. D., Fariñas, I., Sauer, H., Armanini, M., Phillips, H., Reichardt, L. F., Ryan, A. M., Carver-Moore, K., and Rosenthal, A. (1996) Renal and neuronal abnormalities in mice lacking GDNF. *Nature* **382,** 76–79
18. Nakanishi, H., Ogiso, H., and Taguchi, R. (2009) Qualitative and quantitative analyses of phospholipids by LC-MS for lipidomics. *Methods Mol. Biol.* **579,** 287–313
19. Brügger, B., Erben, G., Sandhoff, R., Wieland, F. T., and Lehmann, W. D. (1997) Quantitative analysis of biological membrane lipids at the low picomole level by nanoelectrospray ionization tandem mass spectrometry. *Proc. Natl. Acad. Sci. U.S.A.* **94,** 2339–2344
20. Schliwa, M. (1982) Action of cytochalasin D on cytoskeletal networks. *J. Cell Biol.* **92,** 79–91
21. Sampath, P., and Pollard, T. D. (1991) Effects of cytochalasin, phalloidin, and pH on the elongation of actin filaments. *Biochemistry* **30,** 1973–1980
22. Barak, L. S., Yocum, R. R., and Webb, W. W. (1981) *In vivo* staining of cytoskeletal actin by autointernalization of nontoxic concentrations of nitrobenzoxadiazole-phallacidin. *J. Cell Biol.* **89,** 368–372
23. Strokin, M., Sergeeva, M., and Reiser, G. (2003) Docosahexaenoic acid and arachidonic acid release in rat brain astrocytes is mediated by two separate isoforms of phospholipase A2 and is differently regulated by cyclic AMP and Ca^{2+}. *Br. J. Pharmacol.* **139,** 1014–1022
24. Sanchez-Mejia, R. O., and Mucke, L. (2010) Phospholipase A2 and arachidonic acid in Alzheimer's disease. *Biochim. Biophys. Acta* **1801,** 784–790
25. Lin, T. N., MacQuarrie, R., and Sun, G. Y. (1988) Arachidonic acid uptake by phospholipids and triacylglycerols of rat brain subcellular membranes. *Lipids* **23,** 942–947
26. Holte, L. L., Peter, S. A., Sinnwell, T. M., and Gawrisch, K. (1995) ^2H nuclear magnetic resonance order parameter profiles suggest a change of molecular shape for phosphatidylcholines containing a polyunsaturated acyl chain. *Biophys. J.* **68,** 2396–2403
27. Dai, J., and Sheetz, M. P. (1995) Axon membrane flows from the growth cone to the cell body. *Cell* **83,** 693–701
28. Bruno, M. J., Koeppe, R. E., 2nd, and Andersen, O. S. (2007) Docosahexaenoic acid alters bilayer elastic properties. *Proc. Natl. Acad. Sci. U.S.A.* **104,** 9638–9643
29. Diez, E., and Mong, S. (1990) Purification of a phospholipase A2 from human monocytic leukemic U937 cells: calcium-dependent activation and membrane association. *J. Biol. Chem.* **265,** 14654–14661
30. Boland, L. M., and Drzewiecki, M. M. (2008) Polyunsaturated fatty acid modulation of voltage-gated ion channels. *Cell Biochem. Biophys.* **52,** 59–84
31. Moore, S. A., Yoder, E., Murphy, S., Dutton, G. R., and Spector, A. A. (1991) Astrocytes, not neurons, produce docosahexaenoic acid (22:6 omega-3) and arachidonic acid (20:4 omega-6). *J. Neurochem.* **56,** 518–524
32. Shetty, H. U., Smith, Q. R., Washizaki, K., Rapoport, S. I., and Purdon, A. D. (1996) Identification of two molecular species of rat brain phosphatidylcholine that rapidly incorporate and turn over arachidonic acid *in vivo*. *J. Neurochem.* **67,** 1702–1710
33. Farber, S. A., Slack, B. E., and Blusztajn, J. K. (2000) Acceleration of phosphatidylcholine synthesis and breakdown by inhibitors of mitochondrial function in neuronal cells: a model of the membrane defect of Alzheimer's disease. *FASEB J.* **14,** 2198–2206
34. Sun, G. Y., Xu, J., Jensen, M. D., and Simonyi, A. (2004) Phospholipase A2 in the central nervous system: implications for neurodegenerative diseases. *J. Lipid Res.* **45,** 205–213
35. Hishikawa, D., Shindou, H., Kobayashi, S., Nakanishi, H., Taguchi, R., and Shimizu, T. (2008) Discovery of a lysophospholipid acyltransferase family essential for membrane asymmetry and diversity. *Proc. Natl. Acad. Sci. U.S.A.* **105,** 2830–2835
36. Murakami, M., and Kudo, I. (2002) Phospholipase A2. *J. Biochem.* **131,** 285–292
37. Clark, J. D., Lin, L. L., Kriz, R. W., Ramesha, C. S., Sultzman, L. A., Lin, A. Y., Milona, N., and Knopf, J. L. (1991) A novel arachidonic acid-selective cytosolic PLA2 contains a Ca^{2+}-dependent translocation domain with homology to PKC and GAP. *Cell* **65,** 1043–1051
38. Jenkins, C. M., Han, X., Mancuso, D. J., and Gross, R. W. (2002) Identification of calcium-independent phospholipase A2 (iPLA2)β, and not iPLA2γ, as the mediator of arginine vasopressin-induced arachidonic acid release in A-10 smooth muscle cells: enantioselective mechanism-based discrimination of mammalian iPLA2s. *J. Biol. Chem.* **277,** 32807–32814
39. Quik, M. (1987) Characterization and localization of phospholipase A2 activity in sympathetic ganglia. *J. Neurochem.* **48,** 217–224
40. Morioka, N., Takeda, K., Kumagai, K., Hanada, T., Ikoma, K., Hide, I., Inoue, A., and Nakata, Y. (2002) Interleukin-1β-induced substance P release from rat cultured primary afferent neurons driven by two phospholipase A2 enzymes: secretory type IIA and cytosolic type IV. *J. Neurochem.* **80,** 989–997
41. Hirokawa, N., Niwa, S., and Tanaka, Y. (2010) Molecular motors in neurons: transport mechanisms and roles in brain function, development, and disease. *Neuron* **68,** 610–638
42. Straight, A. F., Cheung, A., Limouze, J., Chen, I., Westwood, N. J., Sellers, J. R., and Mitchison, T. J. (2003) Dissecting temporal and spatial control of cytokinesis with a myosin II Inhibitor. *Science* **299,** 1743–1747
43. Brown, J., and Bridgman, P. C. (2003) Role of myosin II in axon outgrowth. *J. Histochem. Cytochem.* **51,** 421–428
44. Theriot, J. A., Mitchison, T. J., Tilney, L. G., and Portnoy, D. A. (1992) The rate of actin-based motility of intracellular *Listeria monocytogenes* equals the rate of actin polymerization. *Nature* **357,** 257–260
45. Muallem, S., Kwiatkowska, K., Xu, X., and Yin, H. L. (1995) Actin filament disassembly is a sufficient final trigger for exocytosis in nonexcitable cells. *J. Cell Biol.* **128,** 589–598
46. Sontag, J. M., Aunis, D., and Bader, M. F. (1988) Peripheral actin filaments control calcium-mediated catecholamine release from streptolysin-*O*-permeabilized chromaffin cells. *Eur. J. Cell Biol.* **46,** 316–326
47. Kobayashi, H., Maeda, M., and Anraku, Y. (1977) Membrane-bound adenosine triphosphatase of *Escherichia coli*. III. Effects of sodium azide on the enzyme functions. *J. Biochem.* **81,** 1071–1077
48. Hanson, R. M. (2010) Jmol–a paradigm shift in crystallographic visualization. *J. Appl. Crystallogr.* **43,** 1250–1260
49. Ferreri, C., Samadi, A., Sassatelli, F., Landi, L., and Chatgilialoglu, C. (2004) Regioselective *cis-trans* isomerization of arachidonic double bonds by thiyl radicals: the influence of phospholipid supramolecular organization. *J. Am. Chem. Soc.* **126,** 1063–1072